scientific reports

Check for updates

OPEN

The characteristics of multimodal fundus imaging in AMN patients following COVID infection

Wei Qiang[1,2], Lei Zhang[1,2], Ru Wang[1,2], Wei Jia[1,2], Juan Li[1] & Haiyan Wang[1,2]✉

We investigated the features of multimodal fundus imaging in patients with both Coronavirus disease 2019 (COVID-19) and acute macular neuroretinopathy (AMN). This study included 15 patients with 29 eyes, all of whom underwent comprehensive fundus examinations and were followed for 3 months. Based on the diagnosis, patients were categorized into the AMN group and the AMN_PAMM group (AMN combined with paracentral acute middle maculopathy [PAMM]). At baseline, outer nuclear layer (ONL) thickness was not decreased in either group. However, a notable reduction in both outer retinal and full retinal thickness was observed in the AMN_PAMM group but not in the AMN group. Optical coherence tomography angiography (OCTA) demonstrated decreased vessel density (VD) in the intermediate capillary plexus (ICP) and deep capillary plexus (DCP), whereas the VD of the radial peripapillary capillary plexus (RPCP) and superficial vascular plexus (SVP) was increased in both groups. After 3 months of follow-up, ONL thickness and both outer and full retinal thickness were decreased in both groups. The VD of RPCP and SVP showed a significant decrease in the AMN_PAMM group. Visual acuity improvement was observed only in the AMN group, which may be attributed to the increase in choroid vascular index (CVI).

Keywords Acute macular neuroretinopathy (AMN), Coronavirus disease 2019 (COVID-19), Paracentral acute middle maculopathy (PAMM), Optical coherence tomography angiography (OCTA)

Coronavirus disease 2019 (COVID-19), a multi-system disease, results from infection with Severe acute respiratory syndrome coronavirus 2 (SARS-CoV-2). SARS-CoV-2 can attack the cell surface protein angiotensin-converting enzyme 2 (ACE2), which is ubiquitously expressed throughout the body[1]. SARS-CoV-2 infection leads to various ocular manifestations, ranging from mild conjunctivitis to ischemic optic neuropathy[2]. Histological examination shows microvascular thrombus and inflammatory cells in the retinal and choroidal blood vessels of patients who died from COVID-19, similar to those found in the lungs[1,3]. Microvascular thrombosis leads to insufficient blood supply to the retinal capillaries. Patients suffer from ocular complications due to damaged microvascular circulation, such as cotton wool spots, intraretinal hemorrhages, paracentral acute middle maculopathy (PAMM), acute macular neuroretinopathy (AMN), or retinal vein occlusions[4].

Acute macular neuroretinopathy (AMN) is a relatively rare retinal disease[5]. Females are more likely than males to develop AMN[5]. and more than half of the patients develop the disease before age 30[6]. The common and characteristic clinical symptom is paracentral scotomas[6]. The characteristic lesion occurs acutely in the macula. It usually appears as a reddish-brown, wedge-shaped area with its apex pointing toward the fovea of the macula, shaped like a petalloid or tear-drop, often involving the external limiting membrane and photoreceptors[5,6]. On spectral domain optical coherence tomography (SD-OCT), the lesion presents as hyperreflectivity in the outer plexiform layer (OPL) and outer nuclear layer (ONL), with discontinuity of the ellipsoid band and phagosomes zone (PhaZ)[7]. Our knowledge of the disease is mainly derived from case reports[7–9] and lacks long-term follow-up and large-scale statistics. The COVID-19 pandemic has led to a significant increase in the prevalence of AMN[10]. Since the end of 2022, after the COVID-19 pandemic in China, the number of patients with AMN increased significantly. To date, the exact etiology and mechanism remain unknown, but some evidence suggests that it may be due to ischemia of the retinal deep capillary plexus (DCP)[11,12]. However, the changes in retinal and choroidal blood flow in AMN are poorly understood and still controversial. The primary purpose of this study is to further explore retinal changes in AMN patients through multimodal fundus imaging.

[1]Xi'an People's Hospital (Xi'an Fourth Hospital), Shaanxi Eye Hospital, Xi'an 710004, China. [2]Xi'an Key Laboratory of Digital Medical Technology of Ophthalmologic Imaging, Xi'an 710004, China. ✉email: whyeye@126.com

Results

Clinical characteristics

A total of 15 cases with 29 eyes were included in this study, of which 14 patients developed binocular disease. All patients tested positive for COVID-19 nucleic acid testing. Ages ranged from 18 to 52 years with a mean age of 31.33 ± 7.96 years and a median age of 33 years. The onset age was relatively young, with only one patient aged 52 years and the remaining cases aged 18–35 years.

We divided patients into the AMN group and the AMN combined with PAMM group (AMN_PAMM) according to their diagnosis. Patients in the AMN group had an interval of 15 days or less between onset and treatment time. A corresponding control group was selected for each patient at a ratio of 1:1 based on age and sex. The control group had no systemic diseases, refractive abnormalities, glaucoma, fundus diseases, or other eye diseases, and also had no history of eye surgery. A total of 11 patients with 21 eyes were diagnosed with AMN. Four patients (8 eyes) were diagnosed with both AMN and PAMM. After 1 month of follow-up, 9 individuals (18 eyes) were enrolled in the AMN group, and 4 individuals (8 eyes) in the AMN_PAMM group. After 3 months of follow-up, 6 individuals (11 eyes) were enrolled in the AMN group, and 3 individuals (6 eyes) in the AMN_PAMM group (See Table 1).

Systemic concomitant symptom

Patients complained of dark shadow occlusion and blurred vision. All patients exhibited fever, with highest body temperatures ranging from 37.9 to 39.8 ℃. All patients experienced fever prior to the onset of ocular symptoms, and ocular symptoms appeared 1.87 ± 0.81 days after fever. Only one patient exhibited focal lung inflammation. Two patients exhibited systemic inflammatory manifestations; one presented with a slight increase in leukocyte count of 11.90×10^9/L, while another had normal leukocyte levels but elevated C-reactive protein of 8.41 mg/L. Additionally, two patients demonstrated an increase in erythrocyte sedimentation rate (ESR), reaching up to 46 mm/h. Three patients demonstrated elevated levels of plasma fibrinogen, reaching up to 4.68 g/L, while two patients exhibited increased activated partial thromboplastin time (APTT) rising to 41.2 s. Four patients (26.7%) exhibited increased homocysteine (HCY) reaching up to 36.42 μmol/L. One case had a small cerebral ischemic lesion on head MRI (See Table 1).

Ophthalmic examinations

Patients' baseline visual acuity remained satisfactory. The best corrected visual acuity (BCVA) was converted into LogMAR (Logarithm of the Minimum Angle of Resolution). The LogMAR for the AMN group was 0.17 ± 0.21, and for the AMN_PAMM group was 0.13 ± 0.18. The median LogMAR in AMN was 0.097, and in AMN_PAMM was 0.00. Visual acuity in both AMN and AMN_PAMM groups was worse than in the control group ($P < 0.001$). After 1 month of follow-up, the LogMAR visual acuity of the AMN_1mo group showed a mean improvement to 0.030 ± 0.068, and the AMN_PAMM_1mo group was at 0.068 ± 0.16. The median LogMAR in AMN_1mo was 0.00, and in AMN_PAMM_1mo was 0.00. At 3 months of follow-up, the visual acuity in AMN_3mo was 0.022 ± 0.077, and in AMN_PAMM_3mo was 0.061 ± 0.13. The median LogMAR in AMN_3mo was 0.00, and in

	AMN	AMN_PAMM
Number of patients	11	4
Number of eyes	21	8
Age (years), mean ± SD	32.75 ± 7.62	27.50 ± 7.51
Age (years), median	33	29
Sex (M: F)	2:9	2:2
Bilateral	10	4
Time (fever to ocular symptoms(d))	1.8 ± 0.79	1.75 ± 0.96
Time (ocular symptoms to treatment(d))	7 ± 3.49	8.5 ± 5.07
Systemic comorbidities		
Fever(maximum, ℃)	39.0 ± 0.61	39.2 ± 0.60
Pulmonary infection		One case had focal inflammation in lung
Cerebral ischemia		One case had a small cerebral ischemic lesion
Blood test		
Leukocyte(10×10^9/L)	One case increased, maximum 11.90	
hs-CRP (mg/L)	One case increased, up to 8.41	
ESR (mm/h)	two cases increased, maximum 46	
HCY (μmol/L)	Two cases increased, maximum 17.89	Two cases increased, maximum 36.42
TT (s)	One case increased, up to 24.4	
ATPP (s)	One cases increased, maximum 19.1	One case increased, maximum 41.2
Plasma fibrinogen (g/L)	Two cases increased, maximum 4.68	One case increased, maximum 1.63

Table 1. Summary of clinical and demographic characteristics for the present cohort. *hs-CRP* high-sensitivity C-reactive protein; *ESR* erythrocyte sedimentation rate; *HCY* homocysteine; *TT* thrombin time; *ATPP* activated partial thromboplastin time.

AMN_PAMM_1mo was 0.00.After 3 months of follow-up, analysis of visual acuity data indicated a significant improvement in the AMN_1mo and AMN_3mo groups ($P_{AMN} < 0.05$), whereas no significant change was observed in the AMN_PAMM group before and after follow-up ($P_{PAMM} = 0.68$) (See Table 2).

All patients exhibited normal intraocular pressure and no apparent abnormalities in the anterior segment. Dark-reddish lesions could be observed in the macula.

Imaging of the fundus (See Fig. 1)

The lesions exhibited dark-reddish areas in the macular region on color fundus photography (CFP) (See Fig. 1a–d) and scanning laser ophthalmoscopy (SLO) (See Fig. 1e–h). Compared with infrared imaging (IR) (See Fig. 1 i-l), some lesions in CFP appeared unclear and could not be definitively identified. However, cotton wool spots were more distinctly visualized on CFP. In the AMN_PAMM group, 4 eyes (50%) displayed cotton wool spots located no more than 1/2 PD (papillary diameter) on the temporal side of the optic disc. Among them, only one eye displayed superficial retinal hemorrhage in the path of the arteriola temporalis retinae inferior, 1 PD away from the optic disc.

The IR revealed macular hyperreflective lesions with a recognition rate of 100%. These lesions presented in various shapes including palm, wedge, trapezoidal, oval, petal-like, or irregular forms. Confocal scanning laser ophthalmoscopy (cSLO) was utilized for fundus imaging, revealing the lesions with optimal clarity (See Fig. 1 m-p). Lesion area in AMN showed significant variation among individuals, but no statistically significant difference was observed between groups (AMN group was 2.73 ± 2.44 mm^2, AMN_PAMM group was 2.52 ± 2.46 mm^2) (See Fig. 1B). The median lesion area in AMN was 2.61 mm^2, and in AMN_PAMM was 1.79 mm^2.

The minimum lesion area across all groups was 0.064 mm^2, while the maximum reached 7.16 mm^2. Analysis of the quadrants where the lesions were located showed that the quadrant distribution in the AMN group was as follows: S—16 eyes (76.2%), T—8 eyes (38.1%), I—17 eyes (81.0%), N—17 eyes (81.0%). For the AMN_PAMM group, it was: S—8 eyes (100%), T—5 eyes (62.5%), I—7 eyes (87.5%), N—8 eyes (100%). The AMN lesions occurred more frequently in the N quadrant and less frequently in the T quadrant.

After 1 month of follow-up, the lesion area in the AMN_1mo group was 2.93 ± 2.32 mm^2, and in the AMN_PAMM_1mo group was 2.56 ± 2.53 mm^2. The median lesion area in AMN_1mo was 2.29 mm^2 and in AMN_PAMM_1mo was 2.11 mm^2. At 3 months of follow-up, the lesion area in AMN_3mo was 2.38 ± 1.31 mm^{2}and in AMN_PAMM_3mo was 2.45 ± 2.13 mm^2. The median lesion area in AMN_3mo was 1.95 mm^2 and in AMN_PAMM_3mo was 1.78 mm^2. There was no significant difference in lesion area before and after follow-up in both AMN and AMN_PAMM groups.

Fluorescein fundus angiography (FFA) and Indocyanine green angiography (ICGA) (See Fig. 2)

In the AMN group, fluorescein fundus angiography (FFA) showed weak fluorescence in the perifoveal vascular arch region in 4 eyes and mild peripheral macular fluorescence leakage during the late stage of FFA in 2 eyes. Indocyanine green angiography (ICGA) examination revealed weak fluorescence in the macular region in 11 eyes during the late stage of ICGA (See Fig. 2). In the AMN_PAMM group, 6 eyes displayed weak fluorescence in the perifoveal vascular arch region in the FFA, and 2 eyes revealed focal mild leakage around the macula during the late FFA phase, while 1 eye exhibited spot-like transparent fluorescence around the macula. Additionally, ICGA demonstrated weak fluorescence in lesions within the macular area during the late ICGA phase in 6 eyes.

Optical coherence tomography (OCT)

In OCT, the AMN group exhibited hyperreflective signals extending from the outer boundary of the outer plexiform layer (OPL) to the ellipsoid zone (EZ) and the outer segment tips phagocytosed by the pigment epithelium (PhaZ)[13] (See Fig. 3). Scattered spot-like hyperreflective signals were detected within the lesion area in 12 eyes (57.1%). All patients exhibited ellipsoid band and PhaZ discontinuity. All 8 eyes in the AMN_PAMM group exhibited hyperreflective bands extending from the outer boundary of OPL to the PhaZ, as well as hyperreflective bands in the inner nuclear layer (INL) (See Fig. 4). Among them, 4 eyes (50%) displayed cotton wool spots with hyperreflective clumps in nerve fiber layers around the optic disc, involving the ganglion cell layer, accompanied by structural abnormalities affecting all layers of the inner retina. After receiving anti-inflammatory and vasodilator therapy, we conducted a 3-month follow-up and observed the disappearance of hyperreflective bands in both the ONL and INL in the macular region of all patients. The discontinuity of the ellipsoid zone and PhaZ had greatly recovered (See Fig. 3–4).

We measured the thickness of the retina at the macula, including the outer nuclear layer (ONL), outer retina, and full retina, and analyzed the data (See Table 2).

(1) AMN: The thickness of ONL, outer retina, and full retina between the AMN group and control did not exhibit any differences at baseline. At 1 month and 3 months of follow-up, the thickness of the ONL, outer retina, and full retina in the AMN group exhibited a decrease compared to the control group.
(2) AMN_PAMM: In the AMN_PAMM group, the ONL thickness was not decreased at baseline; however, there was a notable reduction in the thickness of both the outer retina and the full retina in the macula. At 1 month and 3 months of follow-up, the thickness of the ONL, outer retina, and full retina in AMN_PAMM groups exhibited a decrease compared to the control group.
(3) Follow-up versus baseline: The thickness of ONL, outer retina, and full retina in the AMN_3mo group was thinner than in the AMN group. The thickness of outer retina and full retina in the AMN_1mo group was thinner than in the AMN group. There were no differences in ONL, outer retina, and full retina thickness between AMN_PAMM_3mo, AMN_PAMM_1mo, and AMN_PAMM.
(4) Comparison between groups: Compared with the AMN group, the outer retina and the full retinal thickness in the macula were significantly thinner in the AMN_PAMM group at baseline. At follow-up of 1 month

	AMN	AMN_1mo	AMN_3mo	AMN_PAMM	AMN_PAMM_1mo	AMN_PAMM_3mo	Control	*P*	P_{1mo}	P_{3mo}	P_{AMN}	P_{PAMM}
LogMAR												
Average	0.17 ± 0.21	0.030 ± 0.068	0.022 ± 0.077	0.13 ± 0.18	0.068 ± 0.16	0.061 ± 0.13	− 0.022 ± 0.032	< 0.001	0.004 < 0.05	0.002 < 0.05	0.005 < 0.05	0.68
Median	0.097	0.00	0.00	0.00	0.00	0.00	0.00					
Lesion area												
Average	2.73 ± 2.44	2.93 ± 2.32	2.38 ± 1.31	2.52 ± 2.46	2.56 ± 2.53	2.45 ± 2.13	–	0.21	0.36	0.082	0.78	0.99
Median	2.61	2.29	1.95	1.79	2.11	1.78	–	–	–	–	–	–
OCT												
ONL thickness	110.80 ± 19.31	98.26 ± 12.39	95.36 ± 8.89	101.25 ± 5.57	97.63 ± 6.48	98.10 ± 10.59	111.43 ± 14.66	0.035 < 0.05	0.002 < 0.05	0.003 < 0.05	0.016	0.59
Outer retina thickness	165.24 ± 18.82	150.17 ± 15.33	147.00 ± 10.38	149.63 ± 12.78	153.25 ± 16.22	147.50 ± 18.01	170.08 ± 11.49	< 0.001	< 0.001	< 0.001	0.010 < 0.05	0.86
Full retina thickness	202.48 ± 22.65	186.33 ± 14.16	183.27 ± 10.41	185.75 ± 10.95	186.88 ± 15.31	182.67 ± 17.17	203.88 ± 14.42	0.005 < 0.05	< 0.001	< 0.001	0.005 < 0.05	0.78

Table 2. LogMAR, lesion and retinal thickness of patients. *ONL* outer nuclear layer; *P* the comparison between AMN, AMN_PAMM and the contorl group at baseline; P_{1mo} the comparison between AMN_1mo, AMN_PAMM_1mo and the contorl group; P_{3mo} the comparison between AMN_3mo, AMN_PAMM_3mo and the contorl group; P_{AMN} the comparison between AMN at baseline, AMN_1mo and AMN_3mo; P_{PAMM} the comparison between AMN_PAMM at baseline, AMN_PAMM_1mo and AMN_PAMM_3mo.

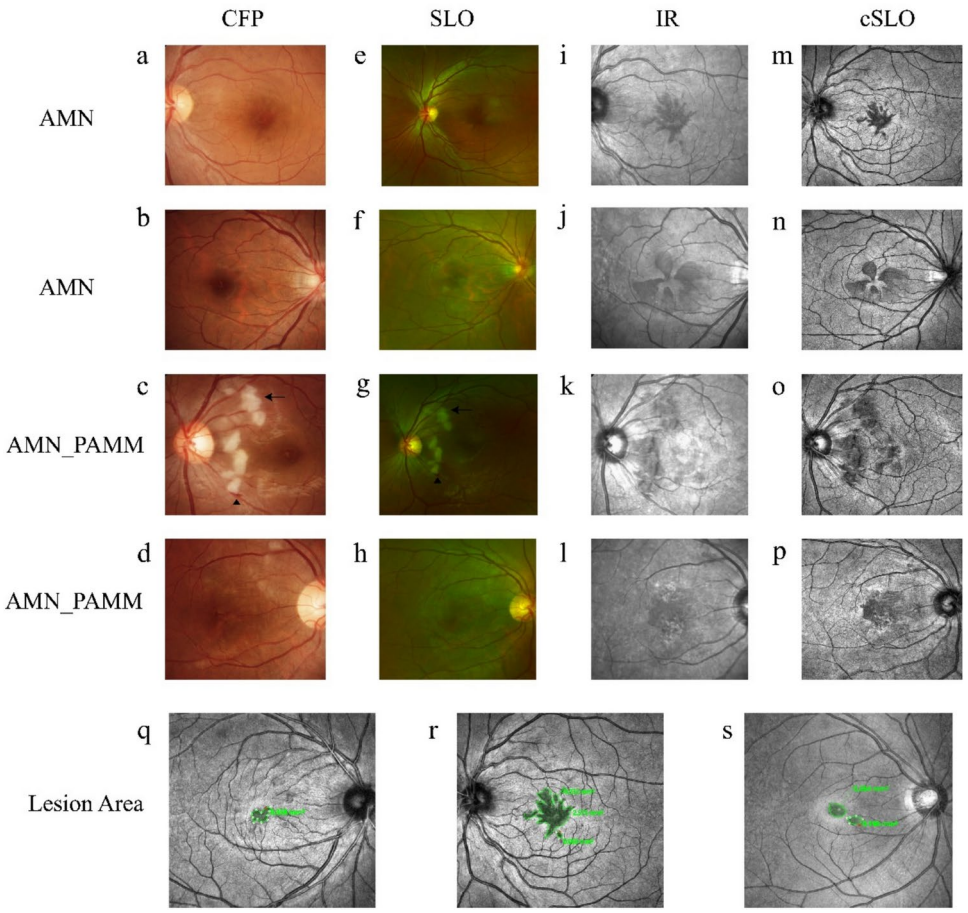

Fig. 1. Fundus photographs of AMN patients. (a–d) Lesions observed in color fundus photography (CFP). (e–h) Scanning laser ophthalmoscopy (SLO) images. (i–l) Infrared fundus photography (IR) images. (m–p) Confocal scanning laser ophthalmoscopy (cSLO). images showing lesions with palm-like, wedge-shaped, trapezoidal, and petal-like characteristics. (q–s) Measurement of lesion area using cSLO.

and 3 months, there were no statistical differences in ONL thickness, outer retinal thickness, and full retinal thickness in the macula among the experimental groups.

Optical coherence tomography angiography (OCTA)

The vascular density (VD) and Choroid vascular index (CVI) was compared between the experimental and control group in the radial peripapillary capillary plexus (RPCP), superficial vascular plexus (SVP), intermediate capillary plexus (ICP), and DCP in ten regions, including 0–1 mm circle, 0–3 mm circle, 0–6 mm circle, 1–3 mm ring, 1–6 mm ring, 3–6 mm ring, 1–6 mm superior quadrant (S), 1–6 mm temporal quadrant (T), 1–6 mm inferior quadrant (I), and 1–6 mm nasal quadrant (N). Vessel density (VD) is defined as the ratio of the area of vascular perfusion to the total area on a binary image. Choroid vascular index (CVI) is defined as the ratio of the medium and large vessel volume of the choroid to the total choroidal volume. Also, we measure the parameters of foveal avascular zone (FAZ) which is a quantitative indicator of blood flow in the fovea. It includes FAZ area, FAZ perimeter, and circularity index (CI) and foveal vessel density (FD): The vascular density (VD) within 300 um of the macular fovea.

Baseline

(1) Vascular density (VD) and Choroid vascular index (CVI) statistics at baseline (See Table 3).

- Comparison between AMN group and Control group: In ICP, the VD was decreased in the 0–3 mm, 0–6 mm circle and 1–3 mm, 1–6 mm, 3–6 mm ring and 1–6 mm (S, N) quadrant; the VD in DCP was decreased in 0–3 mm, 0–6 mm circle and 1–3 mm, 1–6 mm, 3–6 mm ring and 1–6 mm (S, I, N) quadrant. However, the VD was increased in RPCP 0–6 mm circle, 1–6 mm, 3–6 mm ring, 1–6 mm (S, I, N) quadrant, and also in SVP 0–6 mm circle, 1–6 mm ring, 1–6 mm (S, I) quadrant in the AMN group. Choroid vascular index (CVI) revealed no statistically significant differences among the AMN and Control group (See Table 3).

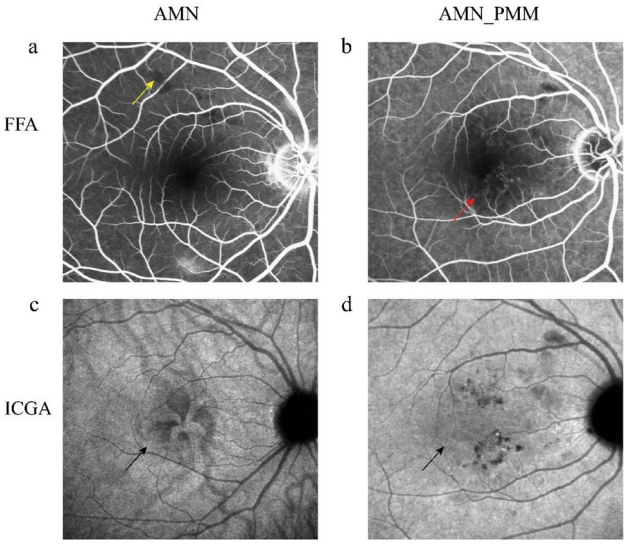

Fig. 2. Fluorescein fundus angiography (FFA) and Indocyanine green angiography (ICGA) of patients. (a, b) FFA of patients. (a) A focal hypoperfusion in the perifoveal vascular arch region arch region (yellow arrow) in FFA in AMN patients. (b) Spot-like transparent fluorescence around the macula (red arrow) in FFA in AMN_PAMM patients. c-d. ICGA of patients. Weak fluorescence at the lesion located in macular area (black arrow) in the late stage of ICGA was observed in AMN and AMN_PAMM groups.

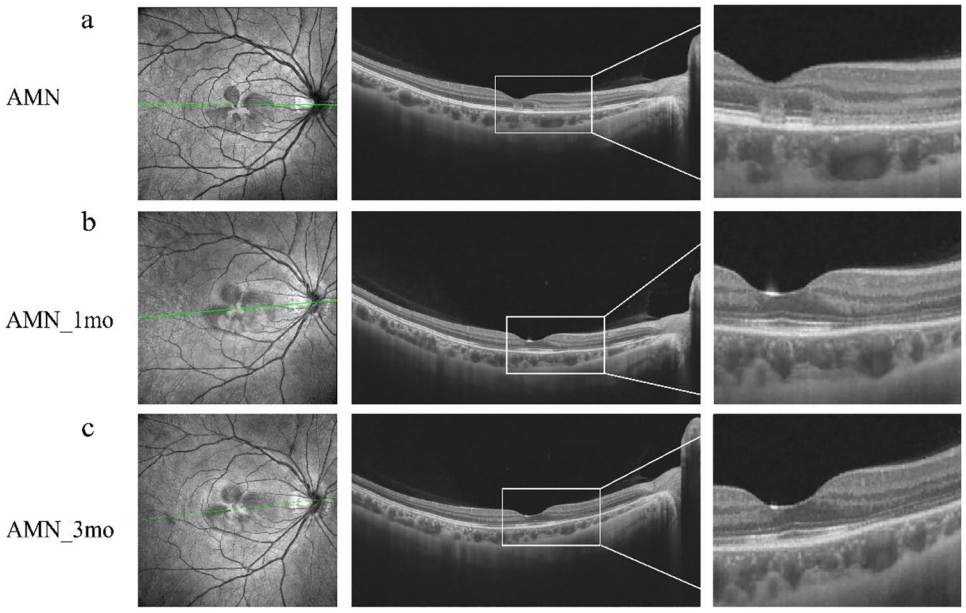

Fig. 3. Optical coherence tomography (OCT) finding in AMN patients. (**a**) At baseline, the AMN group exhibited hyperreflective signals extending from the outer boundary of the outer plexiform layer (OPL) to the ellipsoid zone (EZ) and the outer segment tips phagocytosed by the pigment epithelium (PhaZ) in the OCT. The lesion exhibited ellipsoid band and PhaZ discontinuity. (**b**, **c**) The OCT presentation of AMN at 1mo (**b**) and 3mo (**c**) of follow up. The hyperreflective bands in the the outer nuclear layer (ONL) gradually resolved. The discontinuity of the ellipsoid zone and PhaZ has been had greatly recovered.

- Comparison between AMN_PAMM group and Control group: The VD of the AMN_PAMM group in ICP was decreased in the 1–3 mm ring and 1–6 mm (N) quadrant, and the VD in DCP was decreased in the 1–6 mm (N) quadrant. However, the VD was increased in the AMN_PAMM group compared to the control group in the SVP 3–6 mm ring, 1–6 mm (I) quadrant, and RPCP 0–1 mm circle, 1–6 mm (S) quadrant. Choroid vascular index (CVI) revealed no statistically significant differences among the AMN_PAMM groups, and Control group (See Table 3).

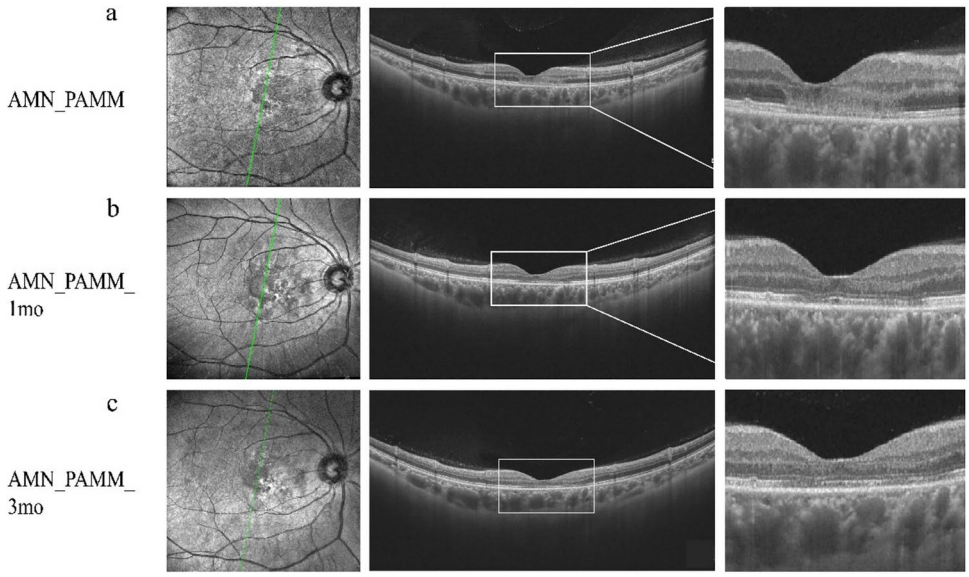

Fig. 4. OCT findings in AMN_PAMM patients. (**a**) At baseline, the hyperreflectivity band extend extends from the outer plexiform layer (OPL) to ellipsoid zone and phagosomes zone (PhaZ), simultaneously appears in the inner nuclear layer (INL). The lesion exhibited discontinuity of ellipsoid band and PhaZ. b-c. The OCT presentation of AMN_PAMM at 1mo (**b**) and 3mo (**c**) of follow up. The disappearance of hyperreflective bands in both the outer nuclear layer (ONL) and INL in the macular region. The discontinuity of the ellipsoid zone and PhaZ has been had greatly recovered but not recovered completed.

(2) FAZ (foveal avascular zone) and Choroid vascular index (CVI).

Statistical analysis of the foveal avascular zone (FAZ), Circularity index (CI), Perimeter (Perim), foveal vessel density (FD) (refers to the vascular density within 300 μm of the macular fovea) revealed no statistically significant differences among the AMN, AMN_PAMM and Control group (See Table 4).

Follow-up for a period of 1 month and 3 months

(1) Vascular density (VD) and Choroid vascular index (CVI) for follow-up (See Table 5)

- Comparison between AMN_1mo group, AMN_3mo and Control group:
  The VD of the AMN_1mo group was decreased in ICP 0–1 mm, 0–3 mm circle, 1–3 mm ring, 1–6 mm (N) quadrant, and in DCP 0–3 mm, 0–6mm circle, 1–3 mm, 1–6mm ring and 1–6 mm (N) quadrant. However, the VD was increased in RPCP 0–6 mm circle, 1–6 mm ring, 3–6 mm ring, and also 1–6 mm (S, I, N) quadrant.
  The VD of ICP was decreased in AMN_3mo in ICP 0–1 mm, 0–3 mm, 0–6 mm circle, 1–3 mm, 1–6 mm, 3–6 mm ring, 1–6 mm (I) quadrant, and the VD of DCP was decreased in DCP 0–3 mm, 0–6 mm circle, 1–3 mm, 1–6 mm ring, 1–6 mm (I, N) quadrant. However, for the VD of RPCP, the AMN_3mo group showed an increase in RPCP 0–6 mm circle, 1–6 mm, 3–6 mm ring, and 1–6 mm (S, I, N) quadrant. The comparison of CVI at follow-up between the AMN group and the control group found no significant difference at follow up (See Table 5).
- Comparison between AMN_PAMM_1mo group, AMN_PAMM_3mo group and Control group:
  The VD of the AMN_PAMM_1mo group was decreased in ICP 0–1 mm, 0–3 mm circle, and 1–3 mm ring, and in DCP 0–3 mm circle, 1–3 mm ring. Also, the VD of AMN_PAMM_1mo in SVP 0–3 mm circle, 1–3 ring was decreased. However, in RPCP 0–1 mm circle, the AMN_PAMM_1mo group showed an increase. The VD of AMN_PAMM_3mo was decreased in ICP 0–1 mm, 0–3 mm circle, 1–3 mm ring, and in DCP 0–3 mm, 0–6 mm circle, 1–3 mm ring, 1–6 mm (I) quadrant. Also, the VD of SVP was decreased in SVP 0–1 mm, 0–3 mm circle, 1–3 mm ring, 1–6 mm (S, T) quadrant. The comparison of CVI at follow-up between the AMN_PAMM group and the control group found no significant difference at follow up (See Table 5).

(2) FAZ (foveal avascular zone) and Choroid vascular index (CVI)at follow-up

Statistical analysis of the FAZ, CI, and Perim revealed no statistically significant differences between pre- and post-follow-up in the three groups. Foveal vessel density (FD) of AMN_1mo and AMN_PAMM_1mo, AMN_PAMM_3mo were lower than in the control group (See Table 6).

Diameter (mm)		AMN	AMN_PAMM	Control	*P*
RPCP					
0–1 mm	Average (%)	0.45 ± 0.63	2.64 ± 2.25	0.49 ± 0.72	0.031 < 0.05
0–3 mm	Average (%)	3.92 ± 1.33	4.01 ± 1.59	3.56 ± 1.48	0.64
0–6 mm	Average (%)	24.11 ± 2.27	21.12 ± 1.17	20.90 ± 3.11	< 0.001
1–3 mm	Average (%)	4.35 ± 1.47	4.19 ± 1.59	3.95 ± 1.67	0.70
1–6 mm	Average (%)	24.80 ± 2.35	21.67 ± 1.17	21.49 ± 3.20	< 0.001
3–6 mm	Average (%)	30.95 ± 2.92	27.14 ± 1.42	26.77 ± 3.79	< 0.001
1–6 mm	S (%)	28.84 ± 4.88	27.02 ± 1.91	23.41 ± 4.16	< 0.001
	T (%)	9.46 ± 1.85	9.34 ± 2.21	9.12 ± 2.08	0.86
	I (%)	30.06 ± 3.47	25.87 ± 4.19	25.75 ± 3.93	0.001 < 0.05
	N (%)	30.67 ± 3.83	23.59 ± 4.06	27.35 ± 6.13	0.004 < 0.05
SVP					
0–1 mm	Average (%)	9.12 ± 5.06	5.98 ± 4.33	7.03 ± 3.41	0.14
0–3 mm	Average (%)	46.01 ± 4.49	40.60 ± 2.65	43.92 ± 5.13	0.022 < 0.05
0–6 mm	Average (%)	45.71 ± 3.79	44.97 ± 2.51	43.08 ± 3.20	0.042 < 0.05
1–3 mm	Average (%)	50.62 ± 4.66	44.93 ± 2.54	48.53 ± 5.50	0.023 < 0.05
1–6 mm	Average (%)	46.77 ± 3.86	46.13 ± 2.70	44.12 ± 3.30	0.046 < 0.05
3–6 mm	Average (%)	45.61 ± 4.47	46.57 ± 3.84	42.83 ± 3.99	0.039 < 0.05
1–6 mm	S (%)	49.13 ± 4.95	48.86 ± 3.87	45.83 ± 4.17	0.047 < 0.05
	T (%)	40.96 ± 5.56	40.15 ± 4.18	37.29 ± 4.92	0.064
	I (%)	47.10 ± 4.18	47.97 ± 4.63	43.73 ± 4.19	0.014 < 0.05
	N (%)	49.85 ± 3.08	47.37 ± 2.44	50.06 ± 3.88	0.15
ICP					
0–1 mm	Average (%)	9.45 ± 6.23	9.96 ± 5.22	13.37 ± 4.64	0.057
0–3 mm	Average (%)	29.21 ± 4.27	31.26 ± 5.40	35.37 ± 4.95	< 0.001
0–6 mm	Average (%)	27.97 ± 3.26	30.26 ± 3.31	32.03 ± 4.01	0.003 < 0.05
1–3 mm	Average (%)	31.68 ± 4.35	33.92 ± 5.53	38.12 ± 5.21	< 0.001
1–6 mm	Average (%)	28.50 ± 3.32	30.87 ± 3.34	32.56 ± 4.06	0.003 < 0.05
3–6 mm	Average (%)	27.54 ± 3.61	29.96 ± 3.23	30.91 ± 4.22	0.020 < 0.05
1–6 mm	S (%)	26.91 ± 3.45	30.81 ± 6.33	32.29 ± 4.70	0.001
	T (%)	36.22 ± 5.32	38.33 ± 2.43	36.78 ± 4.01	0.53
	I (%)	27.51 ± 3.69	29.99 ± 4.08	29.62 ± 5.23	0.23
	N (%)	23.46 ± 5.52	24.80 ± 4.31	31.61 ± 5.76	< 0.001
DCP					
0–1 mm	Average (%)	2.11 ± 2.38	1.63 ± 1.35	3.03 ± 2.84	0.30
0–3 mm	Average (%)	7.34 ± 3.78	8.08 ± 3.04	11.25 ± 4.10	0.005 < 0.05
0–6 mm	Average (%)	13.41 ± 3.78	16.37 ± 2.64	17.03 ± 3.57	0.005 < 0.05
1–3 mm	Average (%)	8.00 ± 4.02	8.89 ± 3.32	12.27 ± 4.41	0.004 < 0.05
1–6 mm	Average (%)	13.74 ± 3.85	16.81 ± 2.72	17.44 ± 3.62	0.005 < 0.05
3–6 mm	Average (%)	15.74 ± 4.18	19.26 ± 2.93	18.98 ± 3.78	0.008 < 0.05
1–6 mm	S (%)	12.54 ± 3.63	16.53 ± 5.21	17.66 ± 4.55	0.001 < 0.05
	T (%)	22.23 ± 7.66	25.80 ± 3.35	23.91 ± 6.16	0.40
	I (%)	13.43 ± 4.18	17.00 ± 2.83	16.20 ± 4.85	0.057
	N (%)	6.86 ± 3.51	8.33 ± 3.21	11.83 ± 4.69	< 0.001
CVI					
0–1 mm	Average (%)	0.39 ± 0.08	0.38 ± 0.07	0.40 ± 0.08	0.74
0–3 mm	Average (%)	0.39 ± 0.07	0.38 ± 0.05	0.41 ± 0.07	0.31
0–6 mm	Average (%)	0.39 ± 0.05	0.38 ± 0.04	0.41 ± 0.06	0.33
1–3 mm	Average (%)	0.39 ± 0.07	0.37 ± 0.05	0.41 ± 0.07	0.27
1–6 mm	Average (%)	0.39 ± 0.05	0.38 ± 0.04	0.41 ± 0.06	0.32

Continued

Diameter (mm)		AMN	AMN_PAMM	Control	*P*
3–6 mm	Average (%)	0.39 ± 0.05	0.38 ± 0.04	0.41 ± 0.05	0.34
1–6 mm	S (%)	0.38 ± 0.06	0.37 ± 0.05	0.40 ± 0.06	0.28
	T (%)	0.37 ± 0.06	0.36 ± 0.04	0.39 ± 0.06	0.37
	I (%)	0.38 ± 0.05	0.37 ± 0.04	0.40 ± 0.06	0.27
	N (%)	0.40 ± 0.07	0.41 ± 0.05	0.43 ± 0.07	0.30

Table 3. The vascular density (VD) and Choroid vascular index (CVI) at baseline in OCTA. *RPCP* peripapillary capillary plexus, *SVP* superficial vascular plexus, *ICP* intermediate capillary plexus, *DCP* deep capillary plexus, *CVI* choroid vascular index; *P* the comparison between AMN, AMN_PAMM and the contorl group at baseline.

	AMN	AMN_PAMM	Control	*P*
FAZ				
Area (mm^2)	0.40 ± 0.11	0.46 ± 0.09	0.41 ± 0.11	0.47
Perim (mm)	2.57 ± 0.34	2.76 ± 0.37	2.57 ± 0.33	0.36
CI	0.76 ± 0.05	0.75 ± 0.07	0.77 ± 0.07	0.86
FD	38.54 ± 6.08	36.18 ± 6.46	41.40 ± 3.20	0.050

Table 4. Foveal avascular zone (FAZ) of patients at baseline. *FAZ* Foveal avascular zone; *CI (circularity index)* a-circularity index; *Perim* perimetry. CI = 4π × area/perimeter2. *FD (Foveal vessel density)*: the vascular density within 300 um of the macular fovea. *P* the comparison between AMN, AMN_PAMM and the contorl group at baseline.

The comparison of VD, FAZ and CVI data between Experimental group and Control group were seen in Table 7 and Fig. 5.

Comparison of VD and CVI between pre- and post-follow-up (see Table 5)

(1) Comparison between AMN, AMN_1mo, and AMN_3mo: The CVI in 0–1 mm, 0–3 mm, 0–6 mm, 1–3 mm, 1–6 mm, 3–6 mm, and 1–6 mm (S, I, N) of the AMN_1mo group and AMN_3mo was greater than in the AMN group. The CVI of AMN_1mo and AMN_3mo showed no significant difference.
(2) Comparison between AMN_PAMM, AMN_PAMM_1mo, and AMN_PAMM_3mo: The VD of the AMN_PAMM_3mo group and AMN_PAMM_1mo in ICP 1–6 mm (N) quadrant was greater than in the AMN_PAMM group. However, in SVP 1–6 mm (S, T) of AMN_PAMM_3mo was lower than in the AMN_PAMM group.

Perimetry

In the AMN group, 2 eyes exhibited paracentral scotoma, 1 eye demonstrated physiological blind spot enlargement, 4 eyes displayed partial quadrant small field defect, and the remaining eyes showed no apparent visual field abnormalities. Perimetry in the AMN_PAMM group revealed paracentral scotoma in one eye and partial quadrants small field defect in three eyes (two of which had annular visual field defects in four quadrants).

After 3 months of follow-up, the majority of patients in the AMN group exhibited recovery of normal visual field. In the AMN_PAMM group, two eyes showed annular visual field defects in four quadrant areas at baseline, with only paracentral scotoma remaining after follow-up.

Statistical analysis was conducted on the mean deviation (MD) and pattern standard deviation (PSD) of the visual field at baseline. The results revealed that the MD values for the AMN group (− 4.37 ± 3.95) and AMN_PAMM group (− 6.80 ± 8.79) in the experimental group were all lower than those of the control group (2.39 ± 1.22), indicating the presence of visual field defects in the experimental group. However, there was no significant difference in PSD between the experimental and control groups.

Electroretinogram (ERG) and visual evoked potential (VEP)

Flash electroretinogram (fERG) and multifocal electroretinogram (mfERG) (see Table 8)

1. AMN group: The amplitude of dark-adapted rod response b-wave (dRod-b) and dark-adapted maximum response b-wave (dMax-b) were increased in the AMN group, with no statistically significant difference observed in light-adapted cone response b-wave (lCone-b) amplitude between the AMN group and control group. There were no significant differences in dark-adapted maximum response a-wave (dMax-a), light-adapted cone response a-wave (lCone-a), and light-adapted 30 Hz flicker response (lFlicker) amplitude compared to the control group. The P1 wave response density of multifocal ERG (mfERG) in the AMN group showed no significance.

Diameter (mm)		AMN_1mo	AMN_3mo	AMN_PAMM_1mo	AMN_PAMM_3mo	P_{1mo}	P_{3mo}	P_{AMN}	P_{PAMM}
RPCP									
0–1 mm	Average (%)	0.22 ± 0.46	0.18 ± 0.41	2.27 ± 1.53	1.55 ± 1.25	0.002 < 0.05	0.051	0.27	0.53
0–3 mm	Average (%)	3.76 ± 1.25	4.54 ± 1.44	4.47 ± 1.97	3.85 ± 1.59	0.34	0.21	0.29	0.78
0–6 mm	Average (%)	24.58 ± 2.31	25.37 ± 2.73	20.39 ± 2.30	20.31 ± 2.63	< 0.001	< 0.001	0.37	0.71
1–3 mm	Average (%)	4.20 ± 1.40	5.09 ± 1.62	4.75 ± 2.09	4.14 ± 1.68	0.50	0.18	0.28	0.77
1–6 mm	Average (%)	25.28 ± 2.37	26.10 ± 2.80	20.93 ± 2.33	20.85 ± 2.70	< 0.001	< 0.001	0.37	0.71
3–6 mm	Average (%)	31.59 ± 2.81	32.43 ± 3.33	25.98 ± 2.67	25.89 ± 3.57	< 0.001	< 0.001	0.41	0.59
1–6 mm	S (%)	29.03 ± 3.32	27.07 ± 3.35	23.32 ± 5.37	21.76 ± 4.94	< 0.001	0.022 < 0.05	0.41	0.081
	T (%)	10.48 ± 2.39	10.71 ± 2.15	10.16 ± 2.46	9.13 ± 1.06	0.16	0.097	0.20	0.61
	I (%)	29.61 ± 3.22	32.85 ± 4.71	25.15 ± 4.23	271.0 ± 4.95	0.003 < 0.05	< 0.001	0.065	0.72
	N (%)	31.93 ± 4.37	33.82 ± 4.91	24.58 ± 3.21	25.13 ± 4.78	0.002 < 0.05	0.004 < 0.05	0.15	0.76
SVP									
0–1 mm	Average (%)	6.93 ± 3.82	6.13 ± 3.08	5.71 ± 5.28	2.84 ± 1.63	0.70	0.022 < 0.05	0.12	0.30
0–3 mm	Average (%)	44.95 ± 3.11	45.01 ± 4.67	39.08 ± 7.67	32.55 ± 9.47	0.026 < 0.05	0.011 < 0.05	0.68	0.33
0–6 mm	Average (%)	45.01 ± 3.86	43.80 ± 4.48	43.55 ± 4.31	37.83 ± 8.83	0.25	0.37	0.44	0.14
1–3 mm	Average (%)	49.71 ± 3.42	49.87 ± 5.07	43.25 ± 8.04	36.27 ± 10.50	0.022 < 0.05	0.013 < 0.05	0.79	0.29
1–6 mm	Average (%)	46.11 ± 4.00	44.89 ± 4.61	44.67 ± 4.36	38.84 ± 9.05	0.26	0.42	0.47	0.14
3–6 mm	Average (%)	45.03 ± 4.69	43.39 ± 5.04	45.12 ± 3.53	39.63 ± 8.72	0.20	0.82	0.45	0.16
1–6 mm	S (%)	48.55 ± 3.61	46.93 ± 4.10	44.70 ± 6.50	38.65 ± 6.89	0.071	0.003 < 0.05	0.40	0.015 < 0.05
	T (%)	39.02 ± 6.42	39.27 ± 6.07	38.46 ± 4.92	30.60 ± 7.78	0.61	0.016 < 0.05	0.56	0.013 < 0.05
	I (%)	46.52 ± 3.88	44.23 ± 11.19	46.55 ± 5.25	43.22 ± 11.19	0.087	0.96	0.19	0.47
	N (%)	50.29 ± 4.29	49.11 ± 5.55	49.22 ± 7.09	42.71 ± 12.12	0.87	0.24	0.76	0.42
ICP									
0–1 mm	Average (%)	9.00 ± 4.62	8.49 ± 3.36	7.61 ± 4.39	6.59 ± 4.00	0.003 < 0.05	0.001 < 0.05	0.88	0.38
0–3 mm	Average (%)	31.01 ± 2.96	30.30 ± 4.98	28.27 ± 4.03	29.92 ± 5.36	< 0.001	0.011 < 0.05	0.38	0.49
0–6 mm	Average (%)	29.95 ± 2.56	28.11 ± 4.26	30.44 ± 2.59	32.93 ± 4.20	0.14	0.026 < 0.05	0.15	0.29
1–3 mm	Average (%)	33.77 ± 3.19	33.02 ± 5.39	30.86 ± 4.08	32.84 ± 5.70	< 0.001	0.018 < 0.05	0.31	0.49
1–6 mm	Average (%)	30.56 ± 2.59	28.68 ± 4.31	31.12 ± 2.56	33.70 ± 4.31	0.17	0.026 < 0.05	0.14	0.27
3–6 mm	Average (%)	29.59 ± 3.24	27.38 ± 4.50	31.22 ± 2.53	33.96 ± 4.37	0.44	0.013 < 0.05	0.16	0.11
1–6 mm	S(%)	31.58 ± 3.76	29.96 ± 6.32	30.99 ± 4.43	32.56 ± 3.86	0.74	0.43	0.05	0.79
	T(%)	35.92 ± 3.36	34.87 ± 6.65	34.27 ± 2.64	37.50 ± 5.35	0.11	0.25	0.77	0.078
	I(%)	27.30 ± 6.28	24.66 ± 4.54	29.39 ± 4.27	32.85 ± 4.59	0.40	0.005 < 0.05	0.079	0.32
	N(%)	27.41 ± 3.87	26.68 ± 6.66	30.81 ± 4.66	32.05 ± 7.22	0.032 < 0.05	0.090	0.058	0.038 < 0.05
DCP									
0–1 mm	Average (%)	1.98 ± 2.12	1.38 ± 1.22	1.14 ± 1.40	1.16 ± 0.97	0.13	0.14	0.64	0.73
0–3 mm	Average (%)	7.12 ± 4.65	7.08 ± 3.12	6.21 ± 2.46	7.57 ± 3.44	0.002 < 0.05	0.009 < 0.05	0.98	0.15
0–6 mm	Average (%)	14.03 ± 3.89	13.69 ± 4.20	16.32 ± 4.61	13.47 ± 3.35	0.056	0.026 < 0.05	0.89	0.97
1–3 mm	Average (%)	7.76 ± 5.02	7.80 ± 3.40	6.85 ± 2.72	7.79 ± 3.81	0.002 < 0.05	0.007 < 0.05	0.98	0.15
1–6 mm	Average (%)	14.38 ± 3.97	14.05 ± 4.30	16.76 ± 4.76	13.90 ± 3.39	0.056	0.028 < 0.05	0.88	0.98
3–6 mm	Average (%)	16.36 ± 4.35	15.93 ± 5.04	19.80 ± 5.76	16.11 ± 2.82	0.094	0.088	0.82	0.78
1–6 mm	S (%)	14.91 ± 4.79	15.72 ± 5.47	17.44 ± 6.83	12.66 ± 2.02	0.21	0.064	0.12	0.42
	T (%)	22.74 ± 7.11	22.48 ± 8.56	21.94 ± 5.26	22.32 ± 4.64	0.72	0.79	0.98	0.23
	I (%)	13.05 ± 5.84	10.81 ± 5.80	15.95 ± 6.91	10.55 ± 4.39	0.19	0.008 < 0.05	0.39	0.70
	N (%)	6.80 ± 2.99	7.22 ± 5.04	11.75 ± 5.53	8.96 ± 4.68	0.001 < 0.05	0.038 < 0.05	0.95	0.31
CVI									
0–1 mm	Average (%)	0.44 ± 0.07	0.46 ± 0.069	0.37 ± 0.07	0.38 ± 0.055	0.070	0.070	0.030 < 0.05	0.98
0–3 mm	Average (%)	0.43 ± 0.06	0.45 ± 0.061	0.37 ± 0.06	0.38 ± 0.047	0.075	0.080	0.010 < 0.05	0.92
0–6 mm	Average (%)	0.43 ± 0.05	0.43 ± 0.044	0.38 ± 0.04	0.38 ± 0.040	0.13	0.11	0.015 < 0.05	0.99
1–3 mm	Average (%)	0.43 ± 0.06	0.45 ± 0.061	0.37 ± 0.06	0.38 ± 0.047	0.079	0.087	0.010 < 0.05	0.90
1–6 mm	Average (%)	0.43 ± 0.05	0.43 ± 0.043	0.38 ± 0.04	0.38 ± 0.039	0.14	0.12	0.016 < 0.05	0.99
Continued									

Diameter (mm)		AMN_1mo	AMN_3mo	AMN_PAMM_1mo	AMN_PAMM_3mo	P_{1mo}	P_{3mo}	P_{AMN}	P_{PAMM}
3–6 mm	Average (%)	0.42 ± 0.05	0.43 ± 0.040	0.38 ± 0.03	0.38 ± 0.037	0.17	0.14	0.020 < 0.05	0.96
1–6 mm	S (%)	0.43 ± 0.05	0.43 ± 0.043	0.38 ± 0.04	0.38 ± 0.036	0.13	0.15	0.026 < 0.05	0.87
	T (%)	0.41 ± 0.05	0.41 ± 0.055	0.36 ± 0.04	0.36 ± 0.045	0.10	0.18	0.089	0.94
	I (%)	0.42 ± 0.05	0.44 ± 0.058	0.37 ± 0.04	0.38 ± 0.040	0.17	0.10	0.008 < 0.05	0.97
	N (%)	0.45 ± 0.06	0.46 ± 0.060	0.41 ± 0.05	0.40 ± 0.049	0.31	0.25	0.028 < 0.05	0.96

Table 5. Vessel density (VD) and Choroid vascular index (CVI) of patients at follow up. *RPCP* peripapillary capillary plexus, *SVP* superficial vascular plexus, *ICP* intermediate capillary plexus, *DCP* deep capillary plexus, CVI: Choroid vascular index. P_{1mo}: The comparison between AMN_1mo, AMN_PAMM_1mo and the Contorl group; P_{3mo}: The comparison between AMN_3mo, AMN_PAMM_3mo and the Contorl group; P_{AMN}: The comparison between AMN at baseline, AMN_1mo and AMN_3mo; P_{PAMM}: The comparison between AMN_PAMM at baseline, AMN_PAMM_1mo and AMN_PAMM_3mo.

	AMN_1mo	AMN_3mo	AMN_PAMM_1mo	AMN_PAMM_3mo	P_{1mo}	P_{3mo}	P_{AMN}	P_{PAMM}
FAZ								
Area (mm^2)	0.43 ± 0.10	0.45 ± 0.089	0.49 ± 0.10	0.50 ± 0.14	0.21	0.15	0.31	0.72
Perim (mm)	2.66 ± 0.43	2.72 ± 0.30	2.94 ± 0.40	2.94 ± 0.62	0.072	0.10	0.42	0.67
CI	0.76 ± 0.09	0.77 ± 0.047	0.71 ± 0.09	0.74 ± 0.089	0.200	0.61	0.91	0.56
FD	36.18 ± 6.09	38.24 ± 4.22	34.22 ± 7.35	28.90 ± 7.74	0.005 < 0.05	< 0.001	0.21	0.18

Table 6. Foveal avascular zone (FAZ) of AMN patients at follow up. *FAZ* Foveal avascular zone; *CI (Circularity index)* a-circularity index. *Perim* perimetry. CI = 4π × area/perimeter2. *FD (Foveal vessel density)* the vascular density within 300 um of the macular fovea. P_{1mo} the comparison between AMN_1mo, AMN_PAMM_1mo and the contorl group; P_{3mo} the comparison between AMN_3mo, AMN_PAMM_3mo and the contorl group; P_{AMN} the comparison between AMN at baseline, AMN_1mo and AMN_3mo; P_{PAMM} the comparison between AMN_PAMM at baseline, AMN_PAMM_1mo and AMN_PAMM_3mo.

	AMN	AMN_1mo	AMN_3mo	AMN_PAMM	AMN_PAMM_1mo	AMN_PAMM_3mo
RPCP	0–6 mm, ↑ 1–6 mm, 3–6 mm, 1–6 mm(S,I,N)	0–6 mm, ↑ 1–6 mm, 3–6 mm, 1–6 mm(S,I,N)	0–6 mm, ↑ 1–6 mm, 3–6 mm, 1–6 mm(S,I,N)	0–1 mm, ↑ 1–6 mm(S)	0–1 mm, ↑	–
SVP	0–6 mm, ↑ 1–6 mm, 1–6 mm(S,I)	–	–	3–6 mm, ↑ 1–6 mm(I)	0–3 mm, ↓ 1–3 mm	0–1 mm, ↓ 0–3 mm, 1–3 mm, 1–6 mm(S,T)
ICP	0–3 mm, ↓ 0–6 mm, 1–3 mm, 1–6 mm, 3–6 mm 1–6 mm(S,N)	0–1 mm, ↓ 0–3 mm, 1–3 mm, 1–6 mm(N)	0–1 mm, ↓ 0–3 mm, 0–6 mm, 1–3 mm, 1–6 mm, 3–6 mm, 1–6 mm(I)	1–3 mm, ↓ 1–6 mm(N)	0–1 mm, ↓ 0–3 mm, 1–3 mm	0–1 mm, ↓ 0–3 mm, 1–3 mm
DCP	0–3 mm, ↓ 0–6 mm, 1–3 mm, 1–6 mm, 3–6 mm, 1–6 mm(S,I,N)	0–3 mm, ↓ 0–6 mm, 1–3 mm, 1–6 mm, 1–6 mm(N)	0–3 mm, ↓ 0–6 mm, 1–3 mm, 1–6 mm, 1–6 mm(I,N)	1–6 mm(N) ↓	0–3 mm ↓ 1–3 mm	0–3 mm, ↓ 0–6 mm, 1–3 mm, 1–6 mm(I)
FAZ	–	FD↓		–	FD↓	FD↓
CVI	–	–	–	–	–	–

Table 7. The comparison of OCTA data between experimental group and control group. *RPCP* radial peripapillary capillary plexus; *SVP* superficial vascular plexus; *ICP* Intermediate capillary plexus; *DCP* deep capillary plexus; *FAZ* Foveal avascular zone; *FD (Foveal vessel density)* the vascular density within 300 um of the macular fovea; *CVI* choroid vascular index.

2. AMN_PAMM group: The amplitude of light-adapted cone response b-wave (lCone-b) and dark-adapted maximum response b-wave (dMax-b) increased in the AMN_PAMM group, while the amplitude of dark-adapted rod response b-wave (dRod-b) exhibited no statistically significant difference between the control group and the AMN_PAMM group. The amplitudes of light-adapted 30 Hz flicker response (lFlicker) and

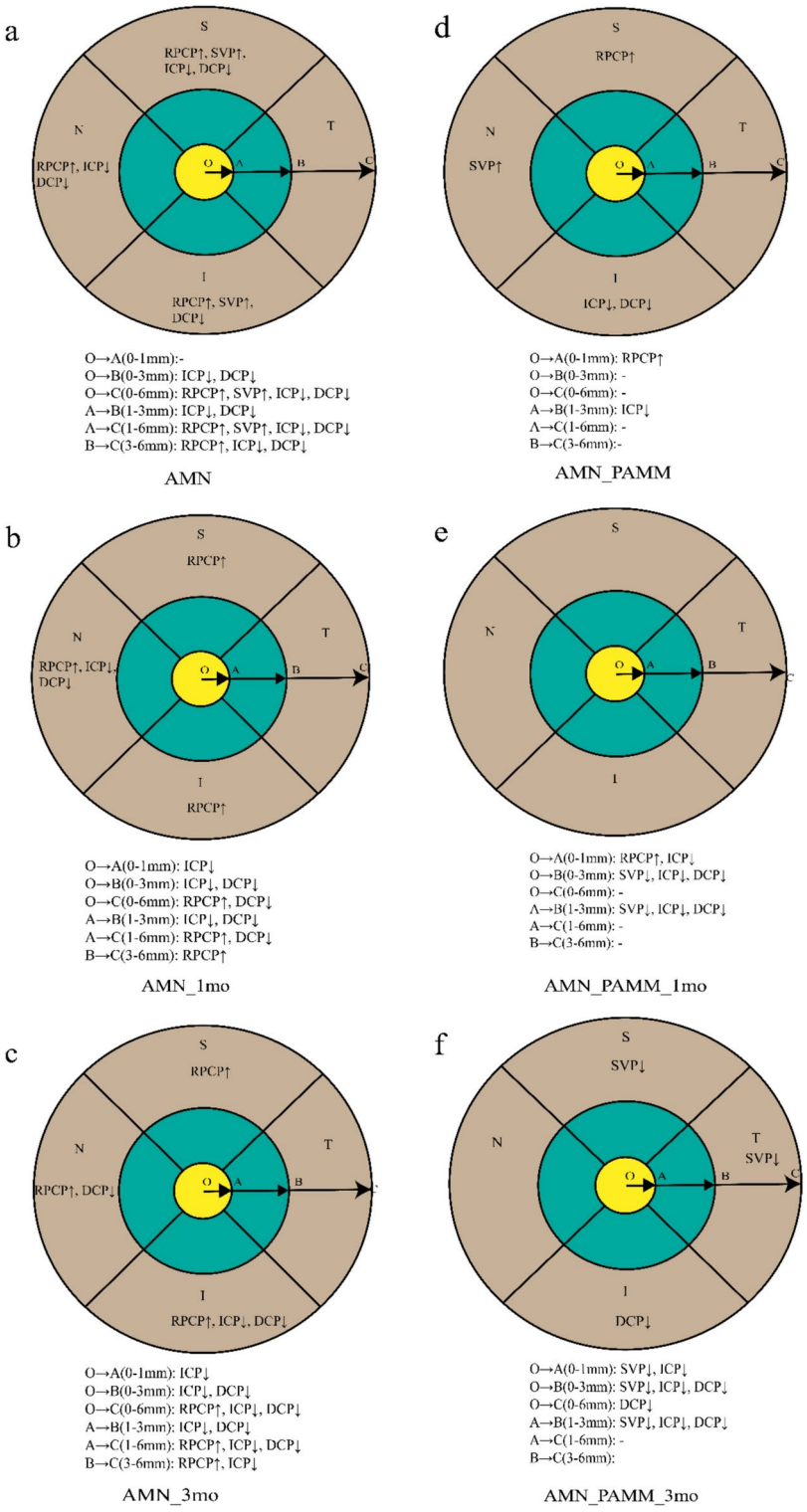

Fig. 5. Vascular density (VD) in AMN and AMN_PAMM patients in OCTA. (**a**–**c**) The VD of AMN patients at baseline (**a**), 1mo of follow up (**b**), 3mo of follow up (**c**). (**d**–**f**) The VD of AMN_PAMM patients at baseline (**d**), 1mo of follow up (**e**), 3mo of follow up (**f**). Different color blocks represent different regions of the macular ETDRS grid. The O represent the macular fovea. O → A represents a circular area of 1 mm radius centered on the macula fovea (yellow block, 0-1 mm). O → B represents a circular area of 3 mm radius centered on the macula fovea (yellow block + green block, 0–3 mm). O → C represents a circular area of 6 mm radius centered on the macula fovea (yellow block + green block + brown block, 0–6 mm). A → B represents a ring area (green block, 1–3 mm). A → C represents a ring area (green block + brown block, 1–6 mm). B → C represents a ring area (brown block, 3–6 mm). We measure VD in the S, T, I, N quadrant in the 1–6 mm ring area and presented it in the macular ETDRS grid. *S* superior, *T* temporal, *I* inferior, *N* nasal, *RPCP* radial peripapillary capillary plexus, *SVP* superficial vascular plexus, *ICP* intermediate capillary plexus, *DCP* deep capillary plexus.

		AMN	AMN_PAMM	Control	*P*
FERG					
dRod-b	Amplitude (uv)	169.70 ± 42.47	143.74 ± 36.30	137.13 ± 29.62	0.034 < 0.05
dMax-b	Amplitude (uv)	372.10 ± 55.01	369.54 ± 29.37	332.66 ± 35.79	0.014 < 0.05
lCone-b	Amplitude (uv)	102.54 ± 22.10	126.69 ± 15.54	101.69 ± 22.80	0.022 < 0.05
dMax-a	Amplitude (uv)	− 148.22 ± 37.64	− 177.21 ± 22.67	− 130.33 ± 33.74	0.006 < 0.05
lCone-a	Amplitude (uv)	− 18.78 ± 8.01	− 17.19 ± 6.39	− 18.44 ± 8.89	0.91
lFlicker	Amplitude (uv)	73.79 ± 19.44	96.84 ± 10.93	75.91 ± 14.59	0.004 < 0.05
Mf-ERG					
1 Ring	P1 (nv/deg2)	59.98 ± 19.91	41.34 ± 16.38	75.24 ± 26.30	0.003 < 0.05
2 Ring	P1 (nv/deg2)	39.55 ± 6.54	34.95 ± 8.92	44.43 ± 10.76	0.041 < 0.05
3 Ring	P1 (nv/deg2)	30.86 ± 5.56	27.58 ± 5.39	26.86 ± 7.02	0.20
4 Ring	P1 (nv/deg2)	18.29 ± 3.90	17.86 ± 4.19	16.21 ± 3.64	0.26
5 Ring	P1 (nv/deg2)	12.96 ± 2.42	12.88 ± 2.19	11.54 ± 2.29	0.16

Table 8. ERG of AMN patients at baseline. *fERG* flash electroretinogram; *mfERG* multifocal electroretinogram; *dRod-b* dark-adapted rod response b-wave; *dMax-b* dark-adapted maximum response b-wave; *lCone-b* light-adapted cone response b-wave; *dMax-a* dark-adapted maximum response a-wave; *lCone-a* light-adapted cone response a-wave; *lFlicker* light-adapted 30 Hz flicker response.

dark-adapted maximum response a-wave (dMax-a) waves increased, with no significant difference observed in light-adapted cone response a-wave (lCone-a) compared to the control group. At the same time, there was a significant decrease in the P1 wave response density of Ring 1 and Ring 2 of multifocal ERG (mfERG) in the AMN_PAMM group, indicating a notable decline in macular function among AMN_PAMM patients. There was no difference in P1 wave response density in Ring 3, Ring 4, and Ring 5 between the AMN_PAMM group and control group.

3. We conducted Pearson correlation analysis between the structural alterations of the patients on OCT and the performance of ERG in the supplementary part (See supplementary Fig. 1). We did not find strong correlation between retinal thickness on OCT and performance of ERG.

Visual evoked potential (VEP)

The flash visual evoked potential (FVEP) results revealed no statistically significant differences in the amplitude and peak time of the P2 wave between the experimental and control groups. Similarly, the pattern visual evoked potential (PVEP) results indicated no significant disparities in the amplitude and peak time of the P100 wave between the experimental and control groups.

Treatment

All patients received hypodermic injection around the superficial temporal artery of compound anisodine injection, as well as anisodamine plus dexamethasone retrobulbar injection, oral Xueshuantong, vincamine, and other medications to promote vascular dilation.

Discussion

The exact etiology and mechanism of AMN remain unknown. Infection, inflammation, and ischemia may be pathogenic factors of AMN. The most common risk factors for AMN are viral flu-like illness or fever (47.5%), use of oral contraceptives (35.6%), and exposure to either epinephrine or ephedrine[5,6], Other factors include leukemia, dengue fever, ulcerative colitis, chronic kidney disease, and others[9]. Research has consistently attributed these risk factors to vascular etiology[6,14].During the COVID-19 epidemic, the incidence of AMN/PAMM increased significantly. Severe acute respiratory syndrome coronavirus 2 (SARS-CoV-2) is the virus responsible for COVID-19, which is a multiorgan disease. ACE2, the receptor of SARS-CoV-2, is located in endothelial cells of arteries and veins and in arterial smooth muscle cells[15]. SARS-CoV-2 binding to ACE2 can down-regulate the expression of ACE2 and its major downstream peptide Ang-(1–7), causing endothelitis, vascular inflammation, and impaired vascular tone[3,15,16]. Patients infected with the virus have a significantly higher incidence of thromboembolic complications, up to 30%[1,17], and microthrombosis is considered a major factor driving disease severity[18]. The ultrastructure of the thrombus includes accumulation of red cells, malformation and hemolysis, fibrin meshworks, and extracellular traps[1,3]. Histological examination of patients who died from COVID-19 revealed microvascular thrombosis and inflammatory cells in the retinal and choroidal vessels[3]. In COVID-19 patients, endothelial damage and micro-thrombosis resulted in capillary plugging and tissue ischemia[18]. It is speculated that the reduction of VD in ICP and DCP is caused by retinal capillary embolism and tissue ischemia in AMN/PAMM patients with COVID-19 due to microvascular thrombosis.

Vessel density (VD) is defined as the ratio of the area of vascular perfusion to the total area on a binary image. The VD decreased because the vascular perfusion area was significantly reduced due to retinal capillary embolism, while the total area remained unchanged. Alexei N. Kulikov et al. found that in AMN eyes, the vessel density of both RPCP, SVP, ICP, and DCP were reduced[19]. Song et al.[20] found voids of vessel signals in the superficial (11.54%), intermediate (82.69%), and deep capillary plexus (98.08%), and in the choriocapillaris

(19.23%) using OCTA. In AMN patients, several studies proved the attenuation of signal or impairment of the DCP in OCTA[21–23]. All these data indicate that the etiology of AMN may be caused by ischemia of ICP and DCP. Our results demonstrated decreasing VD of ICP and DCP in AMN patients, but the VD of SVP and RPCP was increased. It is speculated that the decrease of VD in ICP and DCP leads to a compensatory increase of blood flow in RPCP and SVP. We also included a subset of patients with both AMN and PAMM. Consistent with AMN, PAMM also appeared as a gray lesion with near-infrared reflectance imaging[24]. However, in SD-OCT, the lesions of PAMM are located in the INL[11]. PAMM was associated with retinal vascular diseases such as retinal vascular occlusions, inflammatory chorioretinopathies, congenital glaucoma, foveal hypoplasia, various intraocular and extraocular surgeries, and systemic vascular diseases[5]. Iovino described that PAMM and AMN often occur in eyes with central retinal vein occlusion (CRVO) and Purtscher-like retinopathy[24]. During SARS-CoV-2 infection and vaccination, reports of AMN and PAMM increased significantly[5], however, there were few cases of AMN and PAMM in one eye[25–27]. In our study, we found co-occurrence of AMN and PAMM in the same eye after COVID-19 infection but did not find CRVO and Purtscher-like retinopathy in AMN or PAMM eyes. The presence of PAMM indicates infarction in the INL layer, which is mainly caused by hypoperfusion of DCP[24]. Decreased blood flow in SVP and ICP can be seen in PAMM eyes[28].In our study, patients with both AMN and PAMM exhibited more extensive damage to retinal capillaries, leading to increased ischemic features such as cotton wool spots in 50% of the affected eyes. At the baseline, the area of VD in the AMN group was larger than that in the AMN_PAMM group, which may be attributed to data deviation caused by the small number of cases in the AMN_PAMM group. But at 3 months of follow-up, for patients who suffered from both AMN and PAMM, the area where the VD had decreased expanded over time. Also, the VD of SVP, ICP, and DCP were all decreased.

Several studies demonstrated that in AMN patients, the most common changes in OCT were disruption of EZ, OPL hyperreflectivity, ONL thinning, and Henle's layer hyperreflectivity, and the ONL tends to become thinner as the disease recovers[8,21,29]. In our results, the AMN group exhibited hyperreflective signals extending from the outer boundary of outer plexiform layer (OPL) to the ellipsoid zone (EZ) and the outer segment tips phagocytosed by the pigment epithelium (PhaZ)[13] on OCT. The hyperreflective signal has recently been defined as the OCT angular sign of Henle fiber layer (HFL) hyperreflectivity (ASHH)[30], which specifically revealed a hyperreflective lesion consistent with the angulation of the HFL, extending from the OPL to EZ/PhaZ[30]. HFL is located in the outer two-thirds of OPL and contains bundles of unmyelinated cone and rod axons intermingled with outer Müller cell processes. The ASHH morphology closely mirrors the shape of HFL. In the fovea, ASHH exhibits a distinctly vertical orientation. Within the parafoveal region (2500 μm from the fovea), ASHH gradually aligns with the inclination of HFL and may appear as a band. As eccentricity increases in the perifoveal range (5500 μm from the fovea), HFL slope decreases while ASHH transitions to a more vertical orientation[30].

Some articles have confirmed that OPL/HFL hyperreflective lesions in AMN can manifest within 24 h of onset. Subsequently, the retrograde pathway of photoreceptor disruption extends to ONL, ellipsoid zone, and PhaZ, involving photoreceptor nuclei and inner and outer segments[7,30]. The retrograde pathway of photoreceptor disruption may elucidate the pathogenesis of AMN, with the photoreceptor axons and synaptic terminals being the initial targets for disruption, possibly attributed to damage at the distal end of DCP[23,30].Retinal microvessels and photoreceptor cells are mutually influenced[31]. Photoreceptors serve as the natural boundary between the retina and the choroidal blood vessels, and they are also one of the most energy-intensive regions of the retina[31,32]. The oxygen consumption of photoreceptors is provided by DCP at a rate of 10–15%[33], while the choroid supplies 90–100% of their oxygen needs[34].Conversely, de Gooyer et al.[35] discovered that the loss of photoreceptors may lead to weakening of retinal microvessels. The disruption of photoreceptors further exacerbates the loss of retinal capillaries, ultimately leading to damage of the deep vascular complex (DVC). On the other hand, targeting vascular lesions can also improve photoreceptor survival and visual function even in advanced stages of vision loss[36].

In our results, the nasal quadrant in the parafoveal macular region is more frequently affected in AMN patients, and the VD of the nasal quadrant is more prone to decrease. Vascular abnormalities are also usually observed in the nasal parafoveal quadrant in Behçet's uveitis[37,38]. In Behçet's uveitis, several studies assumed that this phenomenon is attributed to a higher density of unmyelinated nerve fibers with high metabolic demand, which may result in an adequate energy supply from the capillaries[37–39]. AMN patients displayed angular sign of Henle fiber layer (HFL) hyperreflectivity (ASHH) on OCT[7,30] and the location of outer retinal changes associated with DCP ischemia appears to be influenced by the length and orientation of HFL[23].The thickness of nasal HFL is greater than that of the temporal side in the parafoveal region. This may result from the higher photoreceptor and ganglion cell densities in the nasal quadrant[30]. The retinal ganglion cell layer and photoreceptors are the most energy-consuming areas in the retina[31,32,40].The high metabolic energy requirements may make the nasal quadrant more vulnerable to ischemic insult[37].

The energy demand of photoreceptors is substantial, with choroidal blood flow serving as the primary source of energy supply. We measured the CVI of patients in our study. Only in the AMN group, the CVI showed significant increases across all regions, and notably, visual acuity improvements were observed in this particular group among the three groups studied. The possible reason is that the blood supply to photoreceptors is primarily provided by the choroid, and the increase of CVI indicated enhanced choroidal perfusion, which may promote the restoration of photoreceptor function, indicating that improvement of vascular function has positive significance for visual function recovery in patients.

Retinal cell injury stems from a reduction in the thickness of the retinal layers[41]. The thinning of the ONL in OCT suggested injury of photoreceptor cells. In the retina, ACE2 was also found to be mainly distributed in the Müller cells, outer segment of cones, and retinal pigment epithelium[42], thus, the SARS-CoV-2 virus can directly attack the cones and lead to degeneration. Also, the reason for photoreceptor degeneration may result from the disruption of cell homeostasis and the loss of function of key supporting cells, such as retinal pigment epithelium

(RPE) cells, Müller cells, and microglia[43]. In COVID-19 patients, the photoreceptors showed axonal thinning, and Müller cells exhibited a honeycomb-like pattern in the ONL[42]. Müller cells play an important role in photoreceptor survival. Müller cells are located close to photoreceptors and sense ionic gradients and metabolize substances. Furthermore, in the event of photoreceptor degeneration, Müller cells assist in the phagocytosis of photoreceptor cell debris, thereby promoting Müller cell proliferation[43,44]. The degeneration of photoreceptors may be closely associated with the pathological changes of Müller cells, which play a role in regulating retinal blood flow and contributing to the formation of the blood-retinal barrier[42,45]. Activated or ameboid-shaped microglia, which have a tendency to migrate to vascular sites, were also observed in COVID-19 patients[42]. The degeneration of photoreceptors will trigger the activation of microglia, but whether it plays a beneficial or harmful role remains controversial[43]. Finally, the loss of cones and visual function has been demonstrated to be associated with the presence and severity of blood-retina barrier (BRB) leakage[31]. ACE2 has been found to be located in endothelial cells and RPE, which are involved in the formation of the inner and outer retinal barriers[42]. Attacks from the SARS-CoV-2 virus can directly break the inner and outer retinal barriers. The disruption of both the inner and outer barriers of the retina leads to the degeneration of photoreceptors.

Our findings have certain limitations. Firstly, while we hypothesized that the etiology of AMN was ischemic, the potential involvement of inflammatory factors cannot be entirely ruled out. We did not assess inflammation-related markers, such as alterations in the expression of specific inflammatory factors in the vitreous or aqueous humor. Secondly, the follow-up duration is limited. After the resolution of symptoms, there is a significant reduction in follow-up cases, impacting the collection of long-term data. Follow-up management is necessary to further observe the long-term situation of retinal ischemia and photoreceptor atrophy in patients and to provide better treatment and follow-up recommendations. After 3 month of follow-up, the data collected from ERG and VEP are insufficient to further quantify the functional recovery of photoreceptor cells.

In conclusion, in patients with COVID-19, the virus can bind to ACE2 receptors, leading to retinal microvascular thrombosis and inflammation, ultimately resulting in reduced VD of DCP and ICP. Furthermore, injury to the distal end of DCP may result in initial damage to the photoreceptor axons and synaptic terminals, leading to comprehensive destruction of the photoreceptor cell through the retrograde pathway of photoreceptor disruption. After a 3-month follow-up, the extent of photoreceptor degeneration and retinal ischemia gradually decreased without complete recovery. In future studies, extending the observation period is necessary to assess potential recovery from retinal ischemia and photoreceptor degeneration for better disease management suggestions. Due to the rarity of AMN, it is challenging to collect a considerable amount of data. Hence, a multicenter study ought to be carried out so that a larger quantity of data can be gathered to validate the current findings. In addition, since AMN is self-limiting, whether treatment has a positive effect on AMN also requires confirmation by a large amount of data.

Methods

Patients

This retrospective study included 23 patients (total 42 eyes, 19 of whom had bilateral involvement). All patients were recruited from Shaanxi Eye Hospital between December 2022 and June 2023. All patients were followed up for 3 months. Patients were diagnosed with acute macular neuroretinopathy (AMN) with confirmed COVID-19 infection.

Patients with the following ocular disease history were excluded: history of ocular trauma, glaucoma or ocular hypertension, uveitis, refractive media opacity affecting fundus observation, other fundus diseases such as age-related macular degeneration, high myopia retinopathy, central serous chorioretinopathy, history of ocular surgery such as refractive surgery or retinal detachment surgery, and systemic diseases such as diabetes, hypertension, tumors, or coronary heart disease. Our research adhered to the Declaration of Helsinki and was approved by the Ethics Committee of Xi'an People's Hospital/Xi'an Fourth Hospital (protocol n. 20220018). Informed consent was obtained from all patients.

Examination

Multimodal imaging of patients included color fundus photographs (ZEISS VISUCAM224, Germany), spectral-domain Optical Coherence Tomography (OCT) (Heidelberg Spectralis, Heidelberg Engineering, Germany), Swept Source OCT angiography (OCTA) (SS-OCT, VG200D, SVision Imaging, Ltd., China), fundus autofluorescence (FAF) (Optos Daytona P200T, United Kingdom), fluorescein angiography (FA), and indocyanine green angiography (ICGA) (Heidelberg Spectralis, Heidelberg Engineering, Germany). Other ophthalmologic examinations included slit-lamp examination, best-corrected visual acuity (BCVA), intraocular pressure (IOP), ultra-wide field fundus imaging (Optos Daytona P200T, United Kingdom), Humphrey visual field tests (Humphrey Field Analyzer 750i, Carl Zeiss, Germany), and visual electrophysiological examinations (GT-2008V-IV 8.1 system, Gote, Chongqing, China) including pattern visual evoked potential (PVEP), flash VEP (FVEP), flash electroretinogram (FERG), and multifocal ERG (mfERG).

OCT and ERG

The thickness of the outer nuclear layer (ONL) in the fovea was manually measured from OCT images. The ONL at the fovea was defined as the region from the internal limiting membrane (ILM) to the external limiting membrane (ELM). At least two experienced operators used calipers provided with the device to measure the ONL thickness. The thickness of the outer retina and full retina were automatically measured by the software's automatic layer segmentation from OCT images.

We analyzed the amplitude (μV) and peak time (ms) of PVEP P100, the amplitude (μV) and peak time (ms) of FVEP P2, the amplitude (μV) and peak time (ms) of scotopic 3.0 ERG responses b-wave, and the P1 wave response density of mfERG.

OCTA

All patients underwent SS-OCTA using 6 × 6 mm macular raster scans centered on the macula. Vessel density (VD) is defined as the ratio of the area of vascular perfusion to the total area on a binary image. The perfusion area refers to the sum of pixel areas above the measurement threshold on a binary image. Choroid vascular index (CVI) is defined as the ratio of the medium and large vessel volume of the choroid to the total choroidal volume. Foveal avascular zone (FAZ), assessed using 3 × 3 mm macular raster scan mode, is a quantitative indicator of blood flow in the fovea. It includes FAZ area, FAZ perimeter, and Circularity index (CI). Circularity index is calculated as $4\pi \times \text{area/perimeter}^2$. Foveal vessel density (FD) refers to the vascular density within 300 μm of the macular fovea. The ETDRS ring consists of a 1 mm circle centered on the macular center and four quadrants defined by concentric circles 6 mm from the fovea: superior (S), temporal (T), inferior (I), and nasal (N). Poor quality OCTA images (quality score < 7) were excluded. The central wavelength of the device is 1050 nm and the spectral width is 110 nm (range: 990–1100 nm), with a scanning speed of 200,000 A-scans per second[46].

The retina is divided into the Superficial vascular complex (SVC), consisting of the radial peripapillary capillary plexus (RPCP) and superficial vascular plexus (SVP), and the Deep vascular complex (DVC), which includes the intermediate capillary plexus (ICP) and deep capillary plexus (DCP). The boundaries were defined as follows: RPCP (upper boundary 5 μm above inner limiting membrane [ILM], lower boundary at the nerve fiber layer [NFL]/ganglion cell layer [GCL] interface); SVP (upper boundary at the NFL/GCL interface, lower boundary at GCL and lower third of inner plexiform layer [IPL]); ICP (upper boundary at GCL and lower third of IPL, lower boundary at middle of inner nuclear layer [INL]); DCP (upper boundary at middle of INL, lower boundary 25 μm below INL/outer plexiform layer [OPL] interface); choroid (upper boundary 25 μm below Bruch's membrane, lower boundary at the bottom of the choroid) (See Fig. 4a-f).

Statistical analysis

All statistical analyses were performed using SPSS version 27 (Statistical Package for Social Science IBM). Quantitative variables were presented as mean ± standard deviation or median with 95% confidence interval. Differences in data between the three experimental groups and control group were determined by one-way analysis of variance (ANOVA). Post-hoc multiple comparison analysis was conducted using the LSD test. Pearson correlation analysis was conducted between the retinal thickness and the ERG. P values < 0.05 were defined as statistically significant.

Data availability

Data available on request from the authors. The data that support the findings of this study are available on request from the corresponding author, [Haiyan Wang], upon reasonable request.

Received: 19 October 2024; Accepted: 21 April 2025
Published online: 08 May 2025

References

1. Teo, K. Y. C., Invernizzi, A., Staurenghi, G. & Cheung, C. M. G. COVID-19-related retinal micro-vasculopathy—A review of current evidence. *Am. J. Ophthalmol.* **235**, 98–110. https://doi.org/10.1016/j.ajo.2021.09.019 (2022).
2. Nasiri, N. et al. Ocular manifestations of COVID-19: A systematic review and META-analysis. *J. Ophthalmic Vis. Res.* **16**, 103–112. https://doi.org/10.18502/jovr.v16i1.8256 (2021).
3. Negri, E. M. et al. Ultrastructural characterization of alveolar microvascular damage in severe COVID-19 respiratory failure. *J. Appl. Physiol.* **135**, 950–955. https://doi.org/10.1152/japplphysiol.00424.2023 (2023).
4. Zhang, Y. & Stewart, J. M. Retinal and choroidal manifestations of COVID-19. *Curr. Opin. Ophthalmol.* **32**, 536–540. https://doi.org/10.1097/ICU.0000000000000801 (2021).
5. Dutta Majumder, P. & Agarwal, A. Acute Macular neuroretinopathy and paracentral acute middle maculopathy during SARS-CoV-2 infection and vaccination. *Vaccines (Basel)* https://doi.org/10.3390/vaccines11020474 (2023).
6. Bhavsar, K. V. et al. Acute macular neuroretinopathy: A comprehensive review of the literature. *Surv. Ophthalmol.* **61**, 538–565. https://doi.org/10.1016/j.survophthal.2016.03.003 (2016).
7. Fawzi, A. A. et al. Acute macular neuroretinopathy: Long-term insights revealed by multimodal imaging. *Retina* **32**, 1500–1513. https://doi.org/10.1097/IAE.0b013e318263d0c3 (2012).
8. Li, M., Zhang, X., Ji, Y., Ye, B. & Wen, F. Acute macular neuroretinopathy in dengue fever. *JAMA Ophthalmol.* https://doi.org/10.1001/jamaophthalmol.2015.2687 (2015).
9. Munk, M. R. et al. New associations of classic acute macular neuroretinopathy. *Br. J. Ophthalmol.* **100**, 389–394. https://doi.org/10.1136/bjophthalmol-2015-306845 (2016).
10. Azar, G. et al. Did the COVID-19 pandemic increase the incidence of acute macular neuroretinopathy?. *J. Clin. Med.* https://doi.org/10.3390/jcm10215038 (2021).
11. Rahimy, E., Kuehlewein, L., Sadda, S. R. & Sarraf, D. Paracentral acute middle maculopathy: What we knew then and what we know now. *Retina (Philadelphia, Pa.)* **35**, 1921–1930. https://doi.org/10.1097/IAE.0000000000000785 (2015).
12. Rahimy, E. & Sarraf, D. Paracentral acute middle maculopathy spectral-domain optical coherence tomography feature of deep capillary ischemia. *Curr. Opin. Ophthalmol.* **25**, 207–212. https://doi.org/10.1097/ICU.0000000000000045 (2014).
13. Cuenca, N. et al. Interpretation of OCT and OCTA images from a histological approach: Clinical and experimental implications. *Prog. Retin. Eye Res.* https://doi.org/10.1016/j.preteyeres.2019.100828 (2020).
14. Turbeville, S. D., Cowan, L. D. & Gass, J. D. M. Acute macular neuroretinopathy: A review of the literature. *Surv. Ophthalmol.* **48**, 1–11 (2003).
15. Kuriakose, J., Montezano, A. C. & Touyz, R. M. ACE2/Ang-(1–7)/Mas1 axis and the vascular system: Vasoprotection to COVID-19-associated vascular disease. *Clin. Sci. (Lond.)* **135**, 387–407. https://doi.org/10.1042/CS20200480 (2021).
16. Robles, J. P. et al. The spike protein of SARS-CoV-2 induces endothelial inflammation through integrin α5β1 and NF-κB signaling. *J. Biol. Chem.* **298**, 101695. https://doi.org/10.1016/j.jbc.2022.101695 (2022).
17. Helms, J. et al. High risk of thrombosis in patients with severe SARS-CoV-2 infection: A multicenter prospective cohort study. *Intensive Care Med.* **46**, 1089–1098. https://doi.org/10.1007/s00134-020-06062-x (2020).
18. Wadowski, P. P. et al. Microvascular thrombosis as a critical factor in severe COVID-19. *Int. J. Mol. Sci.* https://doi.org/10.3390/ijms24032492 (2023).

19. Kulikov, A. N., Maltsev, D. S. & Leongardt, T. A. Retinal microvasculature alteration in paracentral acute middle maculopathy and acute macular neuroretinopathy a quantitative optical coherence tomography angiography study. *Retin. Cases Brief Rep.* **14**, 343–351. https://doi.org/10.1097/ICB.0000000000000709 (2020).
20. Wei, J. et al. A cross-sectional study of fundus lesion characteristics in patients with acute visual impairment caused by COVID-19 infection. *Sci. Rep.* https://doi.org/10.1038/s41598-024-79509-6 (2024).
21. Feng, H. et al. The characteristics of acute macular neuroretinopathy following COVID-19 infection. *BMC Ophthalmol.* https://doi.org/10.1186/s12886-024-03283-2 (2024).
22. Premi, E. et al. Clinical and diagnostic findings of acute macular neuroretinopathy and paracentral acute middle maculopathy in the COVID-19 era. *Ophthalmologica* **246**, 181–191. https://doi.org/10.1159/000533530 (2023).
23. Cabral, D. et al. Deep capillary plexus features in acute macular neuroretinopathy: Novel insights based on the anatomy of Henle fiber layer. *Invest. Opthalmol. Vis. Sci.* https://doi.org/10.1167/iovs.63.13.4 (2022).
24. Iovino, C. et al. Coincident PAMM and AMN and insights into a common pathophysiology. *Am. J. Ophthalmol.* **236**, 136–146. https://doi.org/10.1016/j.ajo.2021.07.004 (2022).
25. Gascon, P. et al. Covid-19-associated retinopathy: A case report. *Ocul Immunol. Inflamm.* **28**, 1293–1297. https://doi.org/10.1080/09273948.2020.1825751 (2020).
26. Goyal, M., Murthy, S. & Annum, S. Retinal manifestations in patients following COVID-19 infection: A consecutive case series. *Indian J. Ophthalmol.* https://doi.org/10.4103/ijo.IJO_403_21 (2021).
27. Kotian, R., Vinzamuri, S. & Pradeep, T. Bilateral paracentral acute middle maculopathy and acute macular neuroretinopathy following COVID-19 vaccination. *Indian J. Ophthalmol.* https://doi.org/10.4103/ijo.IJO_1333_21 (2021).
28. Chu, S., Nesper, P. L., Soetikno, B. T., Bakri, S. J. & Fawzi, A. A. Projection-resolved OCT angiography of microvascular changes in paracentral acute middle maculopathy and acute macular neuroretinopathy. *Invest. Opthalmol. Vis. Sci.* https://doi.org/10.1167/iovs.18-24112 (2018).
29. Gupta, V., Aggarwal, K., Agarwal, A., Katoch, D. & Sharma, M. Optical coherence tomography angiography features of acute macular neuroretinopathy in dengue fever. *Indian J. Ophthalmol.* https://doi.org/10.4103/ijo.IJO_485_17 (2017).
30. Ramtohul, P., Cabral, D., Sadda, S., Freund, K. B. & Sarraf, D. The OCT angular sign of Henle fiber layer (HFL) hyperreflectivity (ASHH) and the pathoanatomy of the HFL in macular disease. *Prog. Retin. Eye Res.* https://doi.org/10.1016/j.preteyeres.2022.101135 (2023).
31. Ivanova, E., Alam, N. M., Prusky, G. T. & Sagdullaev, B. T. Blood-retina barrier failure and vision loss in neuron-specific degeneration. *JCI Insight* https://doi.org/10.1172/jci.insight.126747 (2019).
32. Yu, D. Y. & Cringle, S. J. Oxygen distribution and consumption within the retina in vascularised and avascular retinas and in animal models of retinal disease. *Prog. Retin. Eye Res.* **20**, 175–208. https://doi.org/10.1016/s1350-9462(00)00027-6 (2001).
33. Birol, G., Wang, S., Budzynski, E., Wangsa-Wirawan, N. D. & Linsenmeier, R. A. Oxygen distribution and consumption in the macaque retina. *Am. J. Physiol. Heart Circ. Physiol.* **293**, H1696–H1704. https://doi.org/10.1152/ajpheart.00221.2007 (2007).
34. Joyal, J. S., Gantner, M. L. & Smith, L. E. H. Retinal energy demands control vascular supply of the retina in development and disease: The role of neuronal lipid and glucose metabolism. *Prog. Retin. Eye Res.* **64**, 131–156. https://doi.org/10.1016/j.preteyeres.2017.11.002 (2018).
35. de Gooyer, T. E. et al. Rod photoreceptor loss in $Rho^{-/-}$ mice reduces retinal hypoxia and hypoxia-regulated gene expression. *Invest. Opthalmol. Vis. Sci.* https://doi.org/10.1167/iovs.06-0646 (2006).
36. Otani, A. et al. Rescue of retinal degeneration by intravitreally injected adult bone marrow-derived lineage-negative hematopoietic stem cells. *J. Clin. Investig.* **114**, 765–774 (2004).
37. Ferreira, B. F. A. et al. OCTA biomarkers and microperimetry features in Behçet's uveitis. *Retina* https://doi.org/10.1097/iae.0000000000003891 (2023).
38. Yan, C. et al. Vascular abnormalities in peripapillary and macular regions of Behcet's uveitis patients evaluated by optical coherence tomography angiography. *Front. Med. (Lausanne)* **8**, 727151. https://doi.org/10.3389/fmed.2021.727151 (2021).
39. Garhofer, G., Werkmeister, R., Dragostinoff, N. & Schmetterer, L. Retinal blood flow in healthy young subjects. *Invest. Ophthalmol. Vis. Sci.* **53**, 698–703. https://doi.org/10.1167/iovs.11-8624 (2012).
40. Tan, P. E. Z. et al. Quantitative confocal imaging of the retinal microvasculature in the human retina. *Investig. Opthalmol. Vis. Sci.* https://doi.org/10.1167/iovs.12-10017 (2012).
41. Su, Q., Dong, J., Zhang, D., Yang, L. & Roy, R. Protective effects of the bilobalide on retinal oxidative stress and inflammation in streptozotocin-induced diabetic rats. *Appl. Biochem. Biotechnol.* **194**, 6407–6422. https://doi.org/10.1007/s12010-022-04012-5 (2022).
42. Albertos-Arranz, H. et al. Microglia activation and neuronal alterations in retinas from COVID-19 patients: Correlation with clinical parameters. *Eye Vis.* https://doi.org/10.1186/s40662-023-00329-2 (2023).
43. Karlen, S. J., Miller, E. B. & Burns, M. E. Microglia activation and inflammation during the death of mammalian photoreceptors. *Annu. Rev. Vis. Sci.* **6**, 149–169. https://doi.org/10.1146/annurev-vision-121219-081730 (2020).
44. Bejarano-Escobar, R., Sánchez-Calderón, H., Otero-Arenas, J., Martín-Partido, G. & Francisco-Morcillo, J. Müller glia and phagocytosis of cell debris in retinal tissue. *J. Anat.* **231**, 471–483. https://doi.org/10.1111/joa.12653 (2017).
45. Bringmann, A. et al. Müller cells in the healthy and diseased retina. *Prog. Retin. Eye Res.* **25**, 397–424. https://doi.org/10.1016/j.preteyeres.2006.05.003 (2006).
46. Zhou, N., Xu, X., Liu, Y., Wei, W. & Peng, X. Appearance of tumor vessels in patients with choroidal osteoma using swept-source optical coherence tomographic angiography. *Front. Oncol.* https://doi.org/10.3389/fonc.2021.762394 (2021).

Acknowledgments

This research was financially supported by the Natural Science Basis Research Plan in Shaanxi Province of China (2024JC-YBQN-0912), the General Research Project of Municipal Health Commission in Xi'an, China (2024yb35), Xi'an Science and Technology Project (24YXYJ0077, 24YXYJ0091) and Bethune Lumitin Research Funding for Young and Middle-aged Ophthalmologists (BJ-LM2021011J), the General Cultivation Project of Municipal Health Commission in Xi'an, China (2024ms18), The Chinese Medicine Research Project of Municipal Health Commission in Xi'an, China (SZJ202406), Research Incubation Fund of Xi'an People's Hospital (Xi'an Fourth Hospital) (ZD-8).

Author contributions

Wei Qiang performed the data analysis and wrote the manuscript. Lei Zhang was responsible for validation. Ru Wang conducted data curation. Wei Jia managed data collection. Juan Li performed formal analysis. Haiyan Wang conceptualized and supervised the project.

Declarations

Competing interests
The authors declare no competing interests.

Additional information
Supplementary Information The online version contains supplementary material available at https://doi.org/10.1038/s41598-025-99442-6.

Correspondence and requests for materials should be addressed to H.W.

Reprints and permissions information is available at www.nature.com/reprints.

Publisher's note Springer Nature remains neutral with regard to jurisdictional claims in published maps and institutional affiliations.